

Article

Vaterite Synthesized by Waste Liquid of Extracting Chitin from Crab Shells and the Mineral Loading for Doxorubicin Hydrochloride

Luting Zhang ¹, Peiyuan Sun ², Xiaochi An ¹, Xingxing Wang ¹, Siying Li ¹ and Bin Lian ^{2,*} ¹ College of Life Sciences, Nanjing Normal University, Nanjing 210023, China² College of Marine Science and Engineering, Nanjing Normal University, Nanjing 210023, China

* Correspondence: bin2368@vip.163.com; Tel.: +86-025-85891050

Abstract: To effectively treat the environmental pollution caused by discarded crab shell, chitin was extracted from discarded crab shells by a combined chemical and biological process. The chitin extraction waste liquid was used to culture bacteria to synthesize biogenic vaterite (BV). The mineral morphology and physico-chemical properties of BV were characterized, and the loading characteristics and adsorption mechanism of doxorubicin hydrochloride (DOX) were investigated. The results showed that chitin could be extracted from crab shells using a combination of chemical and biological methods, and the purity of the extracted chitin reached 89.79%; cultivation of *Bacillus velezensis* using extraction waste liquid can induce the synthesis of stable BV; the maximum drug loading of BV towards DOX was 447.58 mg/g and its adsorption behavior fitted the Freundlich model. The findings provide new information for the processing utilization of waste crab shells and the development of novel drug carriers.

Keywords: crab shell; chitin; waste utilization; biogenic vaterite; drug carrier; doxorubicin hydrochloride



Citation: Zhang, L.; Sun, P.; An, X.; Wang, X.; Li, S.; Lian, B. Vaterite Synthesized by Waste Liquid of Extracting Chitin from Crab Shells and the Mineral Loading for Doxorubicin Hydrochloride. *Minerals* **2022**, *12*, 1608. <https://doi.org/10.3390/min12121608>

Academic Editor: Fabio Nudelman

Received: 10 October 2022

Accepted: 12 December 2022

Published: 14 December 2022

Publisher's Note: MDPI stays neutral with regard to jurisdictional claims in published maps and institutional affiliations.



Copyright: © 2022 by the authors. Licensee MDPI, Basel, Switzerland. This article is an open access article distributed under the terms and conditions of the Creative Commons Attribution (CC BY) license (<https://creativecommons.org/licenses/by/4.0/>).

1. Introduction

The great economic value associated with the production, processing, and sale of crabs in aquatic products makes them one of the most important trade commodities in fishery production in China. People also produce large amounts of crab shell wastes while consuming crabs, which are only in small amounts used for the preparation of catalysts, feed additives, and plant growth regulators [1]; most waste crab shells are, however, buried or discarded and left to rot naturally, resulting in wasted resources and environmental pollution. Therefore, the resource utilization of waste crab shells has received widespread attention.

Studies on the chemical composition of crab shells showed that it contains about 20%–50% CaCO₃, 20%–40% protein, 15%–40% chitin, and small amounts of pigments and lipids. There have been more studies into the waste of crab shells for chitin extraction and purification processes in recent years [2,3], mainly including chemical and biological methods. Among them, a chemical method (acid–alkali extraction method) entails a simple process, a large disposal volume, and can remove calcium carbonate and proteins quickly and adequately, but the discharge of a larger amount of acid–alkali waste generates secondary pollution. Liu et al. (2019) and Zhang et al. (2022), respectively, adopted Luria–Bertani medium containing some Ca²⁺ or waste liquid produced by extraction of chitin to culture microorganisms, which can induce the synthesis of biogenic vaterite (BV) [4,5].

Research shows that vaterite is safe, non-toxic, and porous, so it has potential for application making drug carriers, retaining heavy metals, and so on, which provides new ideas for the utilization of crab shells in the treatment of waste liquids [6,7]. However, Zhang et al. (2022) used a lot of acids and alkali in the extraction process of chitin,

which presented serious environmental safety hazards and were difficult to implement [5]. Microbial fermentation methods have many advantages such as simple operation, mild conditions, low energy consumption, and environmental friendliness [8,9]; however, there are drawbacks, such as insufficient removal of CaCO_3 , the time required, and low purity of extracted chitin [10], which make it difficult to realize in industrial practice. Sedaghat et al. (2016) used *Pseudomonas aeruginosa* to remove calcium carbonate and protein from shrimp processing waste with removal rates of 74.76% and 78.46%, respectively [8]. In addition, Taokaew et al. (2020) compared the chitin properties extracted from crab shells by using chemical and biological methods (utilizing *Bacillus pumilus* fermentation) and found that both were structurally similar with a purity of 86% and 73%, respectively [10]. Hajji et al. (2015) employed *Bacillus subtilis* A26 for fermentation to extract chitin, and the products after fermentation showed that the deproteinization rate and decalcification rate could reach 78.20% and 63.90% [11]. These findings suggest that if the biological extraction is used in combination with the chemical extraction method, the amount of acid and alkali can be greatly reduced and the BV can be produced based on the extraction of chitin, so exploring and expanding the potential of BV application will be an important basis for putting the process into practice.

Calcium carbonate shows many advantages as a drug carrier, which has low toxicity and high biocompatibility [12,13], but it is sensitive to acidic pH environment. The acidic environment in tumor tissue and lysosomes can lead to drug release from the drug carrier [14] and may exhibit good, sustained release and high stability [15,16]. Importantly, calcium carbonate is inexpensive with an estimated cost of only USD \$0.20–0.40 per gram of calcium carbonate [16]. In recent years, it has been applied in biological drug loading [17]. The structure of a drug carrier determines whether a drug molecule can be loaded, and its sustained-release effect. Doxorubicin hydrochloride (DOX), an anthracycline antibiotic with a broad antitumor spectrum and superior performance [18], is widely applied in clinical therapy as an antitumor drug product. However, DOX is toxic to the heart and causes nausea and vomiting, fever and bleeding, gastrointestinal damage, and other side effects [19], so their applied doses per unit time need to be controlled. Drug sustained release systems that utilize carriers for drug delivery have many advantages, such as high efficiency in treatment, reduced toxic side effects, reduced number of drug administrations, and convenient and flexible implementation [20].

In this study, the chitin from waste crab shells was extracted by a combination of chemical and biological methods, and the nutrients and Ca^{2+} in the extracted waste liquid were used as the basis for the synthesis of BV under the induction of *Bacillus velezensis*. Combined with mineral characterization and adsorption experiments, the drug loading and sustained release characteristics of DOX by BV were investigated. This study provides a new idea for the efficient and comprehensive utilization of waste crab shells and the development of new drug carriers.

2. Materials and Methods

2.1. Crab Shell Waste

The crab shells used in this experiment were obtained from *Eriocheir sinensis*, and the origins lie in Gaochun District, Nanjing City, Jiangsu Province. *E. sinensis* crab shells are hard in texture, greenish to translucent in color, and orange-red after cooking. The steamed *E. sinensis* crab shells were washed, dried, and sieved through a 60-mesh sieve to produce the crab shell powder used in this experiment.

2.2. Microorganisms and Culture Conditions

Strains used in this experiment included *Bacillus velezensis* (NCBI accession number NZ-CP037417.1); *Lactocaseibacillus rhamnosus*, was obtained by isolation and purification from commercially available yoghurt, identified by 16S rDNA sequencing; *Bacillus subtilis* was purchased from China Center for Type Culture Collection (CCTCC AB 209260).

A *B. velezensis*, *B. subtilis* seed medium was a solution of the Luria–Bertani medium containing: peptone 10 g/L, sodium chloride 10 g/L, yeast extract 5 g/L, deionized water 1 L, and natural pH. *L. rhamnosus* seed medium was MRS medium (DeMan–Rogosa–Sharpe medium): peptone 10 g/L, beef extract 10 g/L, yeast extract 5 g/L, glucose 5 g/L, sodium acetate 5 g/L, diammonium hydrogen citrate 2 g/L, Tween-80 1 g/L, dipotassium hydrogen phosphate 2 g/L, magnesium heptahydrate 0.2 g/L, manganese sulphate monohydrate 0.05 g/L, deionized water 1 L, and pH 6.8. The culture medium was treated by high-temperature autoclaving (115 °C, 30 min), and the seed solution of all three bacteria was incubated for 10 h (37 °C, 180 rpm).

2.3. DOX and PBS Buffer

DOX was purchased from Shanghai Yuanye Company, Shanghai, China). Hydrochloric acid (HCl) was purchased from Sinopharm Chemical Reagent Co., Ltd., Shanghai, China. PBS buffer solutions (pH = 6) were prepared from 100 mL deionized water, 0.044 g of disodium hydrogen phosphate ($\text{Na}_2\text{HPO}_4 \cdot 12\text{H}_2\text{O}$), 0.1368 g of sodium dihydrogen phosphate ($\text{NaH}_2\text{PO}_4 \cdot 2\text{H}_2\text{O}$), and 0.0585 g of sodium chloride (NaCl). All reagents were of analytical grade.

2.4. Extraction of Chitin from Crab Shells

2.4.1. Demineralization

(1) The crab shell powder was first decalcified by fermentation with *L. rhamnosus* in a system containing glucose 100 g/L, crab shells 50 g/L, and deionized water 1 L. The medium was sterilized at 115 °C for 30 min in a 250 mL triangular flask with 100 mL, and inoculated with 4% *L. rhamnosus* seed solution by volume and fermented in a constant-temperature shaker (37 °C, 100 rpm) for two days. The fermentation was centrifuged at 8000 rpm (5804R centrifuge, Eppendorf, DEU) for 15 min, and the filtrate (precipitate A) and fermentation waste solution (waste liquid A) were collected separately and set aside.

(2) An amount of 0.5 mol/L of hydrochloric acid (HCl) solution was added to the above filter residue (precipitate A) and left for 2 h. An additional amount was 5 mL of HCl solution for each portion of crab shell (5 g) treatment residue (precipitate A). This process removed the previously unremoved calcium carbonate. When the reaction was complete, the filter residue (precipitate B) and the waste solution (waste liquid B) were collected and set aside.

2.4.2. Deproteinization

(1) The decalcified filtrate (precipitate B) was deproteinized by *B. subtilis* fermentation in a high-protease-yielding medium as follow: precipitation B of all described in Section 2.4.1, soluble starch 9.37 g/L, peptone 10.85 g/L, yeast extract 1.67 g/L, manganese sulphate 0.07 g/L, ferrous sulphate 0.07 g/L, magnesium sulphate 0.07 g/L, Tween-20 0.07 g/L, sodium dihydrogen phosphate 3.61 g/L, dipotassium hydrogen phosphate 0.63 g/L, and deionized water 1 L. The medium was sterilized at 115 °C for 30 min in a 250 mL triangular flask with 100 mL and inoculated with 4% *B. subtilis* seed solution by volume and fermented in a constant-temperature shaker (37 °C, 180 rpm) for 2 d. The fermentation was centrifuged at high speed (8000 rpm, 15 min) and the filter residue (precipitate C) and fermentation waste solution (waste liquid C) were collected separately and set aside.

(2) An amount of 50 mL of 1 mol/L NaOH solution was added to the above filter residue (precipitate C) and allow to stand in a water bath at 90 °C for 2 h. This process removed any incomplete proteins, and after the reaction was complete, the filter residue (precipitate D) and the waste solution (waste liquid D) were collected and reserved.

2.4.3. Decolorization

Ten-percent H_2O_2 was added to the collected precipitate D, and the ratio of precipitate D to H_2O_2 was 1:3. The decolorization reaction was completed after standing for 2 h. The precipitate was rinsed with deionized water until the rinsing solution was neutral, filtered and dried to obtain chitin [21].

2.4.4. Identification of Chitin and Calculation of Its Purity and Yield

The organic functional group distribution of extracted chitin was characterized using Fourier Transform Infrared Spectroscopy (FTIR, Bruker, Hyperion 2000, DEU). Chitin was scanned in the spectral range $500\text{--}4000\text{ cm}^{-1}$ at room temperature ($25\text{ }^\circ\text{C}$).

The purity of chitin was calculated using the digestion method combined with the weighing method [22,23]. A certain amount of crude chitin sample was weighed into the digestion tube, 50% NaOH solution was added and the digestion was heated on an electric hot plate at $160\text{ }^\circ\text{C}$ until the product in the reaction solution was clear and then the process was terminated. The crude chitin underwent deacetylation after alkaline digestion to form chitosan. Further, the above alkaline digestion solution was filtered through a cloth funnel and the filter residue collected was rinsed several times with deionized water. This filter residue was dehydrated with 95% ethanol, dried, and weighed. Then the chitosan mass was determined. The purity of chitosan can be calculated as follows.

$$w_1 = [(m_1 - m_0)/m] \times 1.26 \times 100 \quad (1)$$

where, w_1 (%) stands for chitin purity, pure chitin as a percentage of crude chitin; m_1 (g) denotes mass of filter paper and chitosan; m_0 (g) is mass of filter paper; m (g) refers to mass of crude chitin extracted from crab shells; constant 1.26 is the conversion factor that links the relative molecular mass of chitin to that of chitosan [24].

The yield of chitin extracted from crab shells was calculated thus:

$$w_2 = (m \times w_1)/m_2 \quad (2)$$

where, w_2 (%): the yield of chitin; refer to Equation (1), $m \times w_1$ indicates the content of extracted pure chitin; m_2 : the mass of crab shells used for chitin extraction.

2.5. Synthetic Biogenic Minerals

2.5.1. Synthetic BV

The waste liquid for chitin extraction in 2.4 was used to induce the synthesis of biogenic minerals. The culture system was a mixture of waste liquid A, B, C, and D, to which peptone 5 g/L, yeast extract 5 g/L, and NaCl 10 g/L were added, and the pH of the liquid was adjusted to neutral using the alkaline waste liquid from NaOH deproteinization (waste liquid D). The mineralization medium is mainly composed of Ca^{2+} (about 2600 ppm), proteins, polysaccharides, and other organic matter. The medium was sterilized at $115\text{ }^\circ\text{C}$ for 30 min, inoculated with 2% *B. velezensis* seed liquid by volume and fermented in a constant-temperature shaker ($37\text{ }^\circ\text{C}$, 180 rpm) for 5 d. The fermentation was centrifuged (8000 rpm, 15 min) and the precipitate was collected and dried in an oven at $55\text{ }^\circ\text{C}$.

2.5.2. Mineral Characterization

The precipitates were ground and passed through a 200-mesh sieve and observed and characterized by XRD (BTX-526, Olympus, USA), FTIR (Bruker, Hyperion 2000, DEU), TGA-DTA (PerkinElmer, Diamond DMA, USA) (test conditions: from $25\text{ }^\circ\text{C}$ to $1000\text{ }^\circ\text{C}$ at $10\text{ }^\circ\text{C}/\text{min}$ under an N_2 atmosphere) and scanning electron microscopy (SEM)-energy-dispersive X-ray spectrometry (EDS), respectively.

2.6. Drug Loading

2.6.1. Experiments with Different BV Additions

The initial concentration of DOX was set at 2 mg/30 mL in a 30-mL loading system, to which 0.02, 0.05, 0.08, and 0.1 g of BV (The sediments synthesized in 2.5.1 are known to be biogenic vaterite in our pre-experiment and following result) was added, with three replicates in each group. The above adsorption system was mixed thoroughly and shaken at 25 °C for 36 h in a shaker at 200 rpm. After drug loading, the precipitate and supernatant (recorded as supernatant A) were collected by centrifugation (8000 rpm, 15 min). The precipitate was dried to constant mass at 55 °C and dissolved in 9.5 mL HCl solution at pH 1, which completely dissolve vaterite. After that, the solution was centrifuged (recorded as supernatant B). The absorbance of DOX in supernatant A and supernatant B was determined using spectrophotometry. The concentration of DOX was calculated from the standard curve of DOX concentration (Figure S1). The drug loading and encapsulation rate [25,26] were calculated thus:

$$\text{Drug loading (mg/g)} = \frac{C \times V}{M} \quad (3)$$

$$R(\%) = \frac{C_0 - C_e}{C_0} \times 100 \quad (4)$$

where C (mg/L) is the concentration of DOX in the HCl-dissolved precipitate; C_0 (mg/L) is the initial concentration of DOX; C_e (mg/L) is the concentration of DOX in the supernatant of the adsorption system when the adsorption reaches equilibrium; V (L) is the volume of the adsorption system; M (g) is the amount of adsorbent BV added; R represents the drug encapsulation rate.

2.6.2. Experiments with Different Initial DOX Concentrations

In a 30-mL loading system, the drug carrier BV was spiked at 0.02 g and DOX solutions with initial concentrations of 2 mg/30 mL, 10 mg/30 mL, 20 mg/30 mL, and 30 mg/30 mL were added to the system. After drug loading, the precipitate was collected by centrifugation (8000 rpm, 15 min) and the DOX content of the BV loading was calculated according to the method in Section 2.6.1.

Based on the above experimental results, the linearized Langmuir (5) and Freundlich (6) equations were fitted thus:

$$\frac{C_e}{Q_e} = \frac{C_e}{Q_{max}} + \frac{1}{Q_{max}K_L} \quad (5)$$

$$\ln Q_e = \ln K_f + \frac{1}{n} \ln C_e \quad (6)$$

where: Q_{max} (mg/g) is the maximum loading of DOX by the adsorbent; K_L (L/mg) represents the adsorption coefficient of the Langmuir model; Q_e (mg/g) is the unit adsorption amount of DOX adsorbed by BV when adsorption reaches equilibrium; C_e (mg/L) is the concentration of DOX in solution when adsorption reaches equilibrium; K_f (mg/L) denotes the Freundlich equation constant; $1/n$ is the Freundlich adsorption strength constant.

2.6.3. Adsorption Kinetics Experiments

The initial concentration of DOX was set at 2 mg/30 mL in a 30 mL loading system, while 0.02 g BV was added. The system was thoroughly mixed and then shaken at 25 °C and 200 rpm in a shaker. Based on this, the reaction times were set to 0.50 h, 1 h, 1.50 h, 2 h, 2.50 h, 5 h, 12 h, 24 h, 36 h, and 48 h, with three replicates at each time point. Samples were collected by centrifugation (8000 rpm, 15 min) at the above time points and the precipitate was collected, and acid solubilized. The loading and packing rates were calculated according to the method described in Section 2.6.1. The pseudo-first-order kinetic (7) and the pseudo-

second-order kinetic (8) equations were fitted based on the experimental results. The linearized equations of the kinetic model were as follows:

$$\ln(q_e - q) = \ln q_e - k_1 t \quad (7)$$

$$\frac{t}{q_t} = \frac{1}{K_2 q_e^2} + \frac{t}{q_e} \quad (8)$$

where: q_t (mg/g) refers to the unit adsorption of DOX by BV at time t ; q_e (mg/g) is the unit adsorption of DOX by BV when adsorption reaches equilibrium; K_1 (min^{-1}) is the equation constant of the pseudo-first-order kinetic equation, min^{-1} ; K_2 is the (g/mg·min) pseudo-second-order kinetic equation constant.

2.6.4. BV-DOX Mineral Complexes and Their Characterization

The BV-DOX complexes were ground, sieved, observed, and characterized by XRD, FTIR, TGA-DTA, and SEM-EDS, respectively.

2.6.5. Slow-Release Experiments

To simulate the microenvironment of cancer cell growth (pH 6) [27], a PBS buffer at a pH of 6 was prepared. An amount of 0.005 g of BV-DOX mineral complex particles was added to 30 mL of PBS buffer and placed at 37 °C and 120 rpm for drug release. From 12 h after drug release, samples were taken at 24-h intervals. Samples were centrifuged (8000 rpm, 15 min) to collect the supernatant. The DOX concentration in the supernatant was determined and calculated according to the method described in Section 2.6.1. The drug release rate was calculated using the experimental data by Equations (9) and (10) [25,26]:

$$Q_{de} \text{ (mg/g)} = \frac{C_{de} \times V}{M} \quad (9)$$

$$D_e \text{ (%) } = \frac{Q_{de}}{Q_e} \times 100 \quad (10)$$

where: C_{de} (mg/L) is the concentration of DOX in the resolving solution; Q_{de} (mg/g) is the unit release of DOX; V (L) denotes the volume of the resolving solution; M (g) is the mass of BV-DOX in the resolving system; Q_e (mg/g) is the unit load of BV on DOX before resolution; and D_e represents the drug release rate.

3. Results and Discussion

3.1. Chitin Characterization

Chitin ($\text{C}_8\text{H}_{13}\text{O}_5\text{N}$)_n is a large organic molecule; FTIR technique can be used to investigate the characteristic groups of its organic chemical bonds. Comparing the FTIR spectra of this experimental extract with the chitin standard (Figure 1), the chemical structure was found to be consistent. The peak at 3450 cm^{-1} was the absorption peak of O-H stretching vibration, the peak around 2878 cm^{-1} was the absorption peak of -C-H stretching vibration, the amide-I band was at 1654 cm^{-1} , the amide II band was found around 1555 cm^{-1} , the amide-III band was found around 1310 cm^{-1} and the peak around 1092 cm^{-1} was the absorption peak of C-O stretching vibration. These characteristic chitin peaks were intact and well defined [28]. This indicated that chitin was successfully extracted from crab shells without destroying the structure of the chitin.

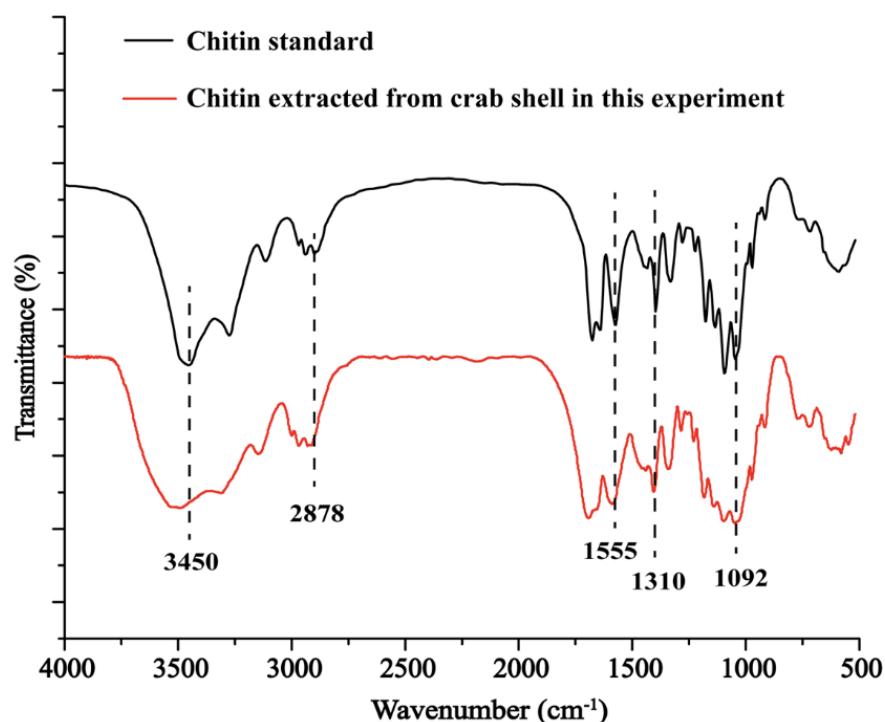


Figure 1. FTIR analysis of chitin extracted from crab shell.

The yield of chitin extracted by combined biological–chemical method was about 17.65% which matched that of report value [29]; however, the purity of chitin extracted by the combined biological–chemical method reached 89.79%, which was significantly higher than that of chitin extracted by the reported chemical and biological methods [30]. The combined biological–chemical method proposed in this study can improve the purity of chitin extracted from crab shells, and the chitin with high purity is of greater application-potential.

3.2. Biogenic Mineral Characterization

Biogenic minerals were synthesized from the waste liquid after the extraction of chitin by using the synthesis method, induced by *B. velezensis*. The mineral composition analysis is illustrated in Figure 2. The XRD result shows that the biogenic mineral induced to form in this experiment is vaterite (ICDD No. 01-1033) (Figure 2a). The FTIR pattern (Figure 2b) indicates that the characteristic vibrational bands at 1406, 1070, and 871 cm^{-1} were caused by CO_3^{2-} . The absorption peaks at 3413 cm^{-1} , 2960 cm^{-1} , 1653 cm^{-1} , and 580 cm^{-1} were vibrational bands of -OH, C-H, C=O, and -SH, respectively. The vibrational bands at 2502 cm^{-1} and 1495 cm^{-1} were -NH-CO-. The TG-DTG results imply that there were three main stages of mass loss (Figure 2c). The first stage (11.5 wt% mass loss) occurred in the temperature range of 25 °C to 269 °C and was mainly caused by evaporation of water from the mineral. The second stage (22.1 wt% mass loss) occurred in the temperature range of 269 to 664 °C, which was mainly caused by the decomposition and combustion of organic matter. The organic matter content in the mineral was about 22.1 wt%. The third stage of mass loss (25.3 wt%) occurred in the temperature range of 664–993 °C, which was caused by the decomposition of CaCO_3 to CaO and CO_2 [6,30]. These results indicate that BV induced by this experiment is a type of organic-inorganic composite mineral material.

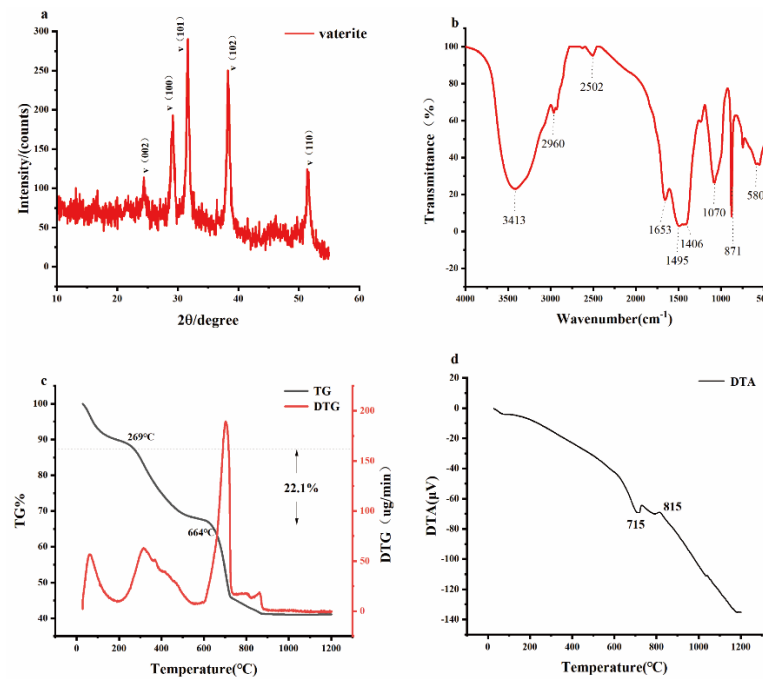


Figure 2. Structural characteristics of BV. (a) XRD pattern. (b) FTIR pattern. (c) TG-DTG curve. (d) DTA curve.

SEM-EDS (Figure 3a,b) can be used for the morphological and elemental composition analysis of the minerals. The results in Figure 3a,b show that the morphology of BV is mostly micro and nano-sized spherical and other irregular aggregate particles. The mineral surface has rough edges and is mainly composed of small nano-particles. EDS spectroscopy indicates that they contain mainly C, O, and Ca (Figure 3c), which further identifies the main composition of the precipitate formed as calcium carbonate.

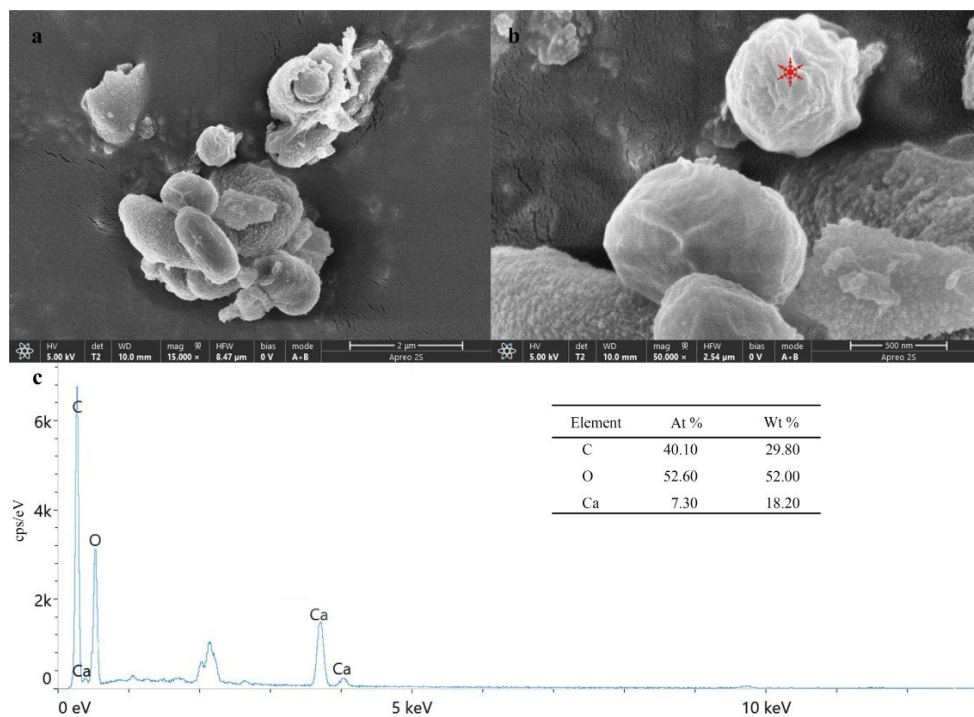


Figure 3. Morphological characteristics in SEM (a,b) and elemental composition analysis of BV by EDS (c).

3.3. Loading and Slow Release of DOX by BV as a Drug Carrier

3.3.1. Effect of BV Addition on Drug Loading of DOX

At the same initial concentration of drug, as higher amounts of BV were added, the encapsulation rate and unit loading of DOX by BV decreased significantly (Figure 4). It may be that the aggregation effect of mineral particles masks some of the adsorption sites on the surface of BV so that the adsorbent cannot make adequate contact with the drug, which in turn affects the adsorption. The highest drug loading (43.7 mg/g) of DOX by BV was achieved when BV was added at 0.02 g.

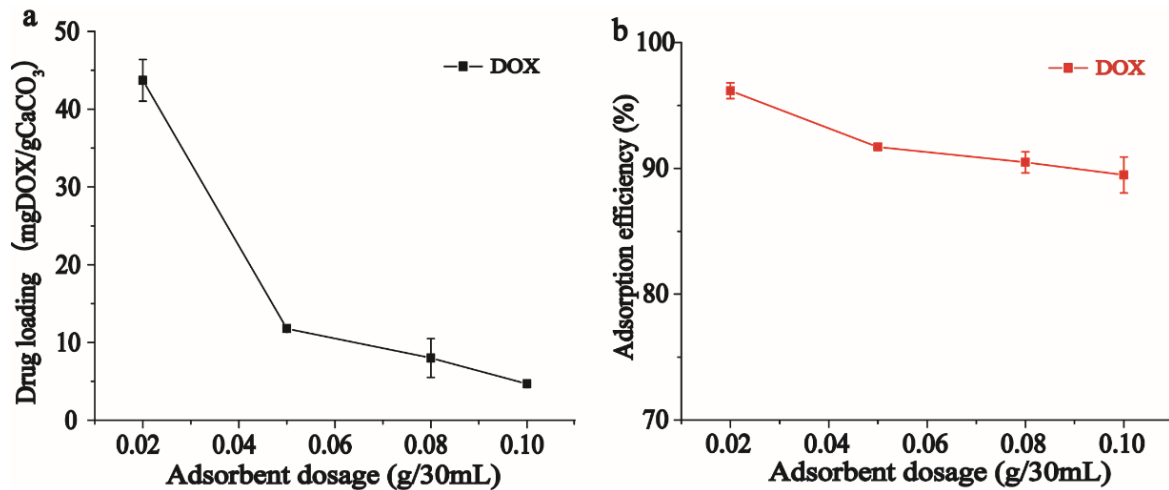


Figure 4. The effect of adsorbent dosage on DOX adsorption using BV. (a) Drug loading. (b) Efficiency of drug encapsulation.

3.3.2. Isotherm Analysis of BV Adsorption on DOX

Based on the above analysis, a BV addition of 0.02 g was chosen for the subsequent DOX adsorption isotherm analysis. In the range of DOX concentration from 2 mg/30 mL to 20 mg/30 mL, the drug loading capacity of BV on DOX increased with increasing initial concentration of DOX (Figure 5a). When the initial concentration of DOX increased again, the drug load of BV on DOX tended to be stable, and the drug load reached 447.58 mg/g. The reason for this result is that all the binding sites on the mineral surface have been occupied. The results in Figure 5b show that the encapsulation rate of DOX by BV decreased as the initial concentration of DOX increased, and this result was related to the aggregation effect between the mineral particles. The results of the adsorption experiments were fitted by linear regression of the adsorption isotherm model (Table 1), which showed that the adsorption of DOX by BV could be better fitted by the Freundlich equation ($R^2 = 0.95$), indicating that the loading behavior of DOX by BV entails multi-molecular layer adsorption.

Table 1. Isotherm parameters according to the Langmuir and Freundlich models.

	Langmuir			Freundlich		
	Q_{max}	K_L (L/mg)	R^2	LnK_f (L/mg)	$1/n$	R^2
DOX	447.58	11.17	0.27	8.67	0.99	0.95

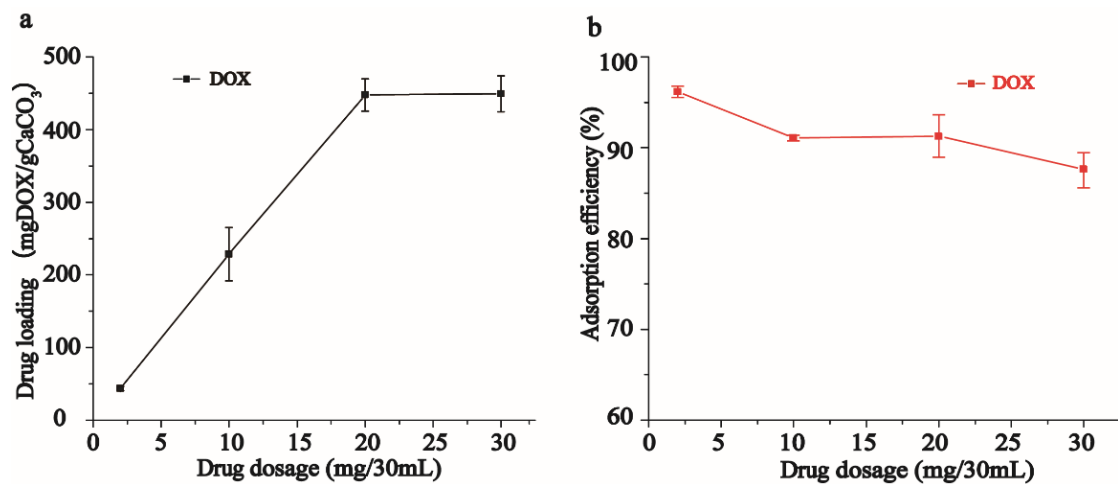


Figure 5. Effect of initial drug concentration on DOX adsorption. (a) Drug loading. (b) Efficiency of drug encapsulation.

3.3.3. Kinetic Analysis of the Adsorption of BV on DOX

DOX adsorption kinetics were performed under the conditions of drug carrier BV addition of 0.02 g and the initial DOX concentration (20 mg/30 mL) according to the analysis described in Section 3.3.2. Under these conditions, the loading of DOX by BV could be increased by extending the duration of the drug loading process (Figure 6). The results showed that the drug loading of DOX by BV increased continuously during the loading process from 0 h to 36 h of adsorption time and reached equilibrium at 36 h, when the drug loading of DOX by BV was stabilized at 447.58 mg/g. In this study, the drug loading of BV on DOX was much higher than that reported so far [31,32], and its drug loading was 396.8 mg/g and 198.5 mg/g, respectively. The results indicated that the BV synthesized in this study had a greater drug loading capacity, which may be related to the specific surface structure of BV [33].

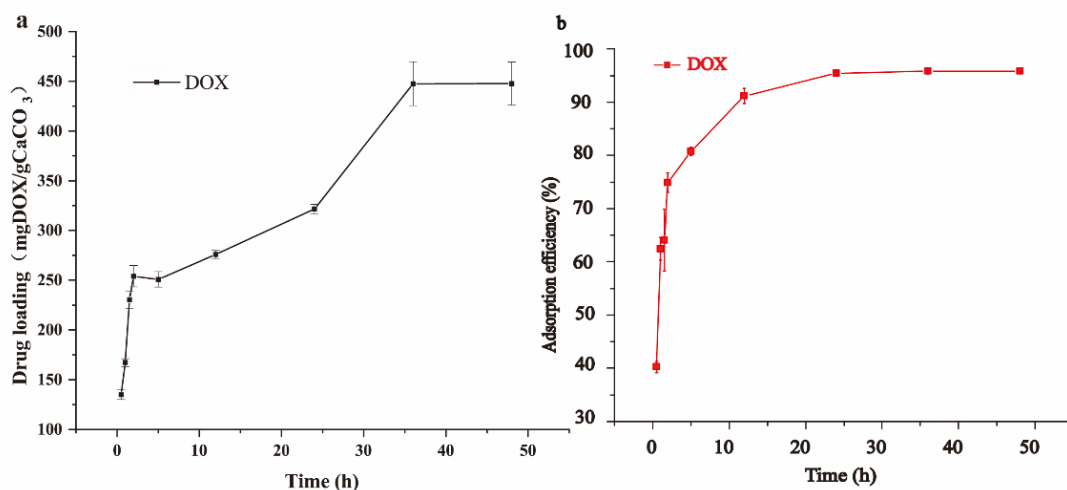


Figure 6. Effect of different times on DOX adsorption. (a) Drug loading. (b) Efficiency of drug encapsulation.

The pseudo-first-order and pseudo-second-order adsorption kinetic models were used to study the DOX adsorption by BV, and the corresponding kinetic parameters were calculated (Table 2). The results showed that the adsorption of DOX by BV was better fitted by the pseudo-second-order kinetic model ($R^2 = 0.96$), indicating that the adsorption of DOX by BV was chemisorption accompanied by some physical adsorptions.

Table 2. Pseudo-first-order and pseudo-second-order adsorption kinetic constants.

	Pseudo-First-Order Kinetic Equations			Pseudo-Second-Order Kinetic Equations		
	q_e	K_1	R^2	q_e	K_2	R^2
DOX	447.58	439.96	0.92	447.58	0.00	0.96

3.3.4. Morphological and Structural Analysis of BV-DOX Mineral Complexes

The optimum loading conditions were obtained according to the analyses described in Sections 3.3.1–3.3.3: in a 30-mL loading system, BV was added at 0.02 g, the initial concentration of DOX was 20 mg/30 mL, and the adsorption time was 36 h. The morphological observation and structural characterization of the BV-DOX mineral complex particles formed in this loading system are illustrated in Figure 7. The SEM-EDS results showed that the surface of BV-DOX was rougher than that of BV, probably due to the attachment of DOX on the surface of BV (Figure 7a–d). Further analysis shows that the FTIR spectra of BV-DOX had some new peaks at 1285 cm^{-1} and 989 cm^{-1} , all of which belonged to DOX characteristic peaks [34] (Figure 7f). The SEM-EDS and FTIR analysis results confirmed that BV can encapsulate DOX.

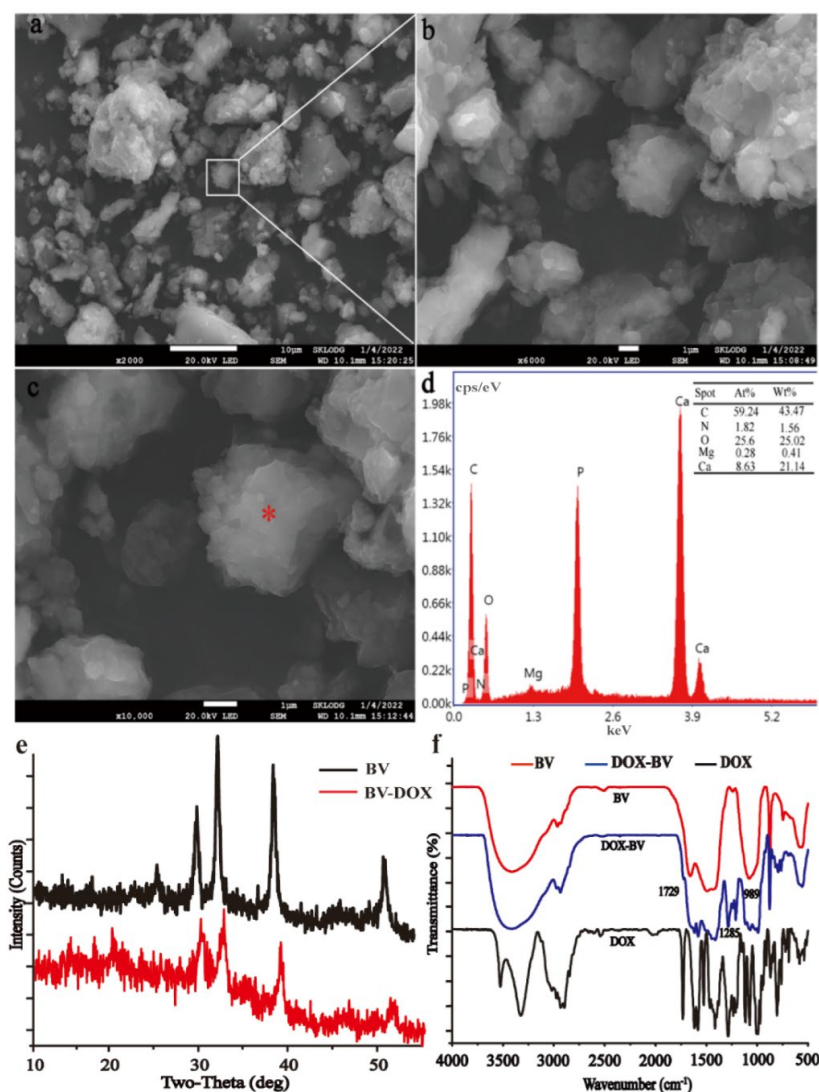


Figure 7. Characteristics and analysis of the BV-DOX mineral complex by using SEM (a–c), EDS (d), XRD (e), FTIR (f).

In the BV-DOX mineral complex, the characteristic FTIR and XRD peaks of BV were still significantly found (Figure 7e,f), indicating that BV can remain stable during particle drying and drug loading. BV mineral surface is rich in negatively charged organic functional groups such as hydroxyl carboxyl groups and mesopores (Figure 2b). It may contribute to the surface loading of DOX by BV through physico-chemical interactions (Table 2).

3.3.5. Analysis of the Retarding Effect of BV on DOX

In a simulated tumor extracellular fluid (pH 6) environment, BV-DOX showed slow-release properties, with DOX release reaching a plateau at 156 h (Figure 8). That suggests that the BV-DOX mineral complex possesses the slow-release function of DOX. The drug release rate of BV was generally consistent with other reported calcium carbonate drug carrier materials [31,32], but the amount of drug release was correspondingly greater due to the superior drug loading capacity of BV, whereby BV could significantly enhance the strength of DOX acting on lesions. Further fitting of the experimental data over the 12–156 h period revealed that the slow release of DOX was uniform over time. The results indicated that the BV-DOX mineral complex has a homogeneous slow release of DOX. The combination of DOX and BV in the BV-DOX mineral complex and the mesoporous distribution of BV may also be associated with the slow release of DOX.

Just to be clear, although the above results show that BV is a good drug carrier and has good slow-release effect, its physiological safety of BV still needs further investigation.

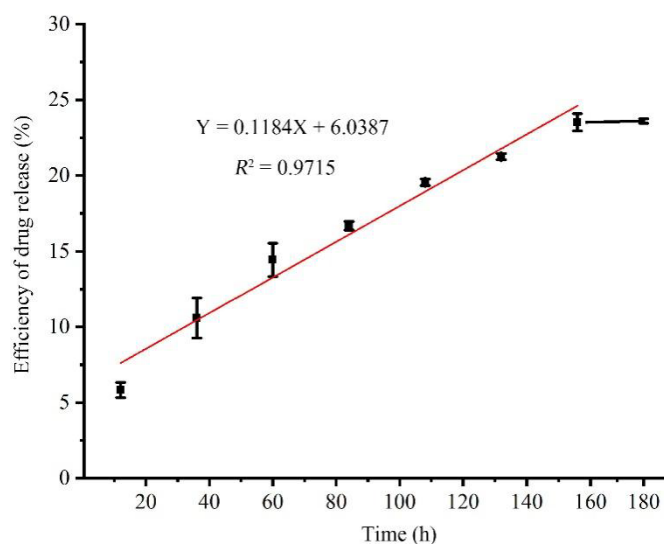


Figure 8. Release rates of loading drugs at different times.

4. Conclusions

In summary, the new extraction processes that combine chemistry and biology methods are used to extract chitin. Micro- and nano-sized vaterite minerals were synthesized by the fermentation culture with *B. velezensis* by using the waste liquid for the extraction of chitin as the medium. This BV exhibited excellent loading properties for DOX with maximum unit drug loading up to 447.58 mg/g; the adsorption of DOX by BV was physico-chemical adsorption of the multiple layers. In simulated tumor extracellular fluid pH (6.0) environment, BV was confirmed to have good sustained-release performance for DOX. This study provides basic information for the application of BV as a novel drug carrier, and offers a new idea for deep-seated development of discarded crab shell resources. However, the biosafety of the biogenic vaterite as a drug carrier still needs further investigation.

Supplementary Materials: The following supporting information can be downloaded at: <https://www.mdpi.com/article/10.3390/min12121608/s1>, Figure S1: Standard curve of DOX.

Author Contributions: Conceptualization, B.L.; Data curation, L.Z. and P.S.; Formal analysis, L.Z., X.W. and B.L.; Investigation, L.Z. and P.S.; Methodology, B.L. and L.Z.; Validation, L.Z. and P.S.; Visualization L.Z., P.S., X.A., X.W. and S.L.; Writing—original draft preparation, L.Z., P.S. and X.A.; Writing—review and editing, B.L., P.S., X.A., X.W. and S.L. All authors have read and agreed to the published version of the manuscript.

Funding: This work was supported by the Interdisciplinary Project of Nanjing Normal University [grant number 164320H1847].

Data Availability Statement: Not applicable.

Conflicts of Interest: The authors declare that they have no conflict of interest.

References

1. Hamed, I.; Özogul, F.; Regenstein, J.M. Industrial applications of crustacean by-products (chitin, chitosan, and chitooligosaccharides): A review. *Trends Food Sci. Technol.* **2016**, *48*, 40–50. [[CrossRef](#)]
2. Ding, H.; Lv, L.; Wang, Z.; Liu, L. Study on the “Glutamic Acid-Enzymolysis” process for extracting chitin from crab shell waste and its by-product recovery. *Appl. Biochem. Biotechnol.* **2020**, *190*, 1074–1091. [[CrossRef](#)] [[PubMed](#)]
3. Ri, G.; Ri, O.S.; Pang, M.R. The function of the crab shell powder as calcium supplementary in the treatment of rickets. *Pediatr. Med.* **2020**, *3*, 6. [[CrossRef](#)]
4. Liu, R.L.; Lian, B. Non-competitive and competitive adsorption of Cd²⁺, Ni²⁺, and Cu²⁺ by biogenic vaterite. *Sci. Total Environ.* **2019**, *659*, 122–130. [[CrossRef](#)] [[PubMed](#)]
5. Zhang, L.; Li, X.; Wang, X.; Lian, B. A study on the extraction of chitin from crab shells and the synthesis of vaterite using the residual waste liquid. *Acta Mineralog. Sin.* **2022**, *42*, 675–682.
6. Dou, J.; Zhao, F.; Fan, W.; Chen, Z.; Guo, X. Preparation of non-spherical vaterite CaCO₃ particles by flash nano precipitation technique for targeted and extended drug delivery. *J. Drug Deliv. Sci. Technol.* **2020**, *57*, 101768. [[CrossRef](#)]
7. Lin, P.Y.; Wu, H.M.; Hsieh, S.L.; Li, J.S.; Dong, C.; Chen, C.W.; Hsieh, S. Preparation of vaterite calcium carbonate granules from discarded oyster shells as an adsorbent for heavy metal ions removal. *Chemosphere* **2020**, *254*, 126903. [[CrossRef](#)]
8. Sedaghat, F.; Yousefzadi, M.; Toiserkani, H.; Najafipour, S. Chitin from *penaeus merguensis* via microbial fermentation processing and antioxidant activity. *Int. J. Biol. Macromol.* **2016**, *82*, 279–283. [[CrossRef](#)]
9. Sedaghat, F.; Yousefzadi, M.; Toiserkani, H.; Najafipour, S. Bioconversion of shrimp waste *Penaeus merguensis* using lactic acid fermentation: An alternative procedure for chemical extraction of chitin and chitosan. *Int. J. Biol. Macromol.* **2017**, *104*, 883–888. [[CrossRef](#)]
10. Taokaew, S.; Zhang, X.; Chuenkaek, T.; Kobayashi, T. Chitin from fermentative extraction of crab shells using okara as a nutrient source and comparative analysis of structural differences from chemically extracted chitin. *Biochem. Eng. J.* **2020**, *159*, 107588. [[CrossRef](#)]
11. Hajji, S.; Ghorbel-Bellaaj, O.; Younes, I.; Jellouli, K.; Nasri, M. Chitin extraction from crab shells by *Bacillus bacteria*. biological activities of fermented crab supernatants. *Int. J. Biol. Macromol.* **2015**, *79*, 167–173. [[CrossRef](#)]
12. Cavallaro, G.; Lazzara, G.; Fakhrullin, R. Mesoporous inorganic nanoscale particles for drug adsorption and controlled release. *Ther. Deliv.* **2018**, *9*, 287–301. [[CrossRef](#)]
13. Paravastu, V.K.K.; Yarraguntla, S.R.; Suvvari, A. Role of nanocomposites in drug delivery. *GSC Biol. Pharm. Sci.* **2019**, *8*, 094–103. [[CrossRef](#)]
14. Wei, W.; Ma, G.H.; Hu, G.; Yu, D.; Mcleish, T.; Su, Z.G.; Shen, Z.Y. Preparation of hierarchical hollow CaCO₃ particles and the application as anticancer drug carrier. *J. Am. Chem. Soc.* **2008**, *130*, 15808–15810. [[CrossRef](#)] [[PubMed](#)]
15. Wang, J.; Chen, J.-S.; Zong, J.-Y.; Zhao, D.; Li, F.; Zhuo, R.-X.; Cheng, S.X. Calcium carbonate/carboxymethyl chitosan hybrid microspheres and nanospheres for drug delivery. *J. Phys. Chem. C* **2010**, *114*, 18940–18945. [[CrossRef](#)]
16. Volodkin, D.V.; von Klitzing, R.; Möhwald, H. Pure protein microspheres by calcium carbonate templating. *Angew. Chem. Int. Edit.* **2010**, *49*, 9258–9261. [[CrossRef](#)] [[PubMed](#)]
17. Sudareva, N.N.; Popryadukhin, P.V.; Suvorova, O.M.; Yukina, G.Y.; Sukhorukova, E.G. Morphology of rat muscle tissue after implantation of delivery systems consisting of porous CaCO₃ vaterites doped with dextran sulfate and containing doxorubicin. *Cell Tiss. Biol.* **2022**, *16*, 392–399. [[CrossRef](#)]
18. Curcio, M.; Brindisi, M.; Cirillo, G.; Frattaruolo, L.; Leggio, A.; Rago, V.; Nicoletta, F.P.; Cappello, A.R.; Iemma, F. Smart lipid-polysaccharide nanoparticles for targeted delivery of doxorubicin to breast cancer cells. *Int. J. Mol. Sci.* **2022**, *23*, 2386. [[CrossRef](#)]
19. Yu, J.; Wang, C.; Kong, Q.; Wu, X.; Lu, J.J.; Chen, X. Recent progress in doxorubicin-induced cardiotoxicity and protective potential of natural products. *Phytomedicine* **2018**, *40*, 125–139. [[CrossRef](#)]

20. Zhang, Y.; Li, L.; Tang, F.; Ren, J. Controlled drug delivery system based on magnetic hollow spheres/polyelectrolyte multilayer core-shell structure. *J. Nanosci. Nanotechnol.* **2006**, *6*, 3210–3214. [[CrossRef](#)]
21. Hisham, F.; Maziati Akmal, M.H.; Ahmad, F.B.; Ahmad, K. Facile extraction of chitin and chitosan from shrimp shell. *Mater. Today Proc.* **2021**, *42*, 2369–2373. [[CrossRef](#)]
22. Wattenberg, L.W.; Patterson, S.; Antonides, J.D. Chitin or chitin-like glycans as targets for late-term cancer chemoprevention. *Cancer Prev. Res.* **2010**, *3*, 1519–1522. [[CrossRef](#)]
23. Kumar, R.; Kaur, N.; Kamilya, D. Chitin modulates immunity and resistance of *Labeo rohita* (Hamilton, 1822) against gill monogeneans. *Aquaculture* **2019**, *498*, 522–527. [[CrossRef](#)]
24. Tang, Q.F.; Wu, Z.T.; Wang, Q.; Jing, T.; Wu, S.L. Preliminary study on chitin content of *Eupolyphaga sinensis* walker. *J. Econ. Anim.* **2004**, *8*, 102–104.
25. Abdallah, M.M.; Ahmad, M.N.; Walker, G.; Leahy, J.J.; Kwapinski, W. Batch and continuous systems for Zn, Cu, and Pb metal ions adsorption on spent mushroom compost biochar. *Ind. Eng. Chem. Res.* **2019**, *58*, 7296–7307. [[CrossRef](#)]
26. Franklin, A.M.; Williams, C.; Andrews, D.M.; Watson, J.E. Sorption and desorption behavior of four antibiotics at concentrations simulating wastewater reuse in agricultural and forested soils. *Chemosphere* **2022**, *289*, 133038. [[CrossRef](#)]
27. Chen, C.; Bai, L.; Cao, F.; Wang, S.; He, H.; Song, M.; Chen, H.; Liu, Y.; Guo, J.; Si, Q.; et al. Targeting LIN28B reprograms tumor glucose metabolism and acidic microenvironment to suppress cancer stemness and metastasis. *Oncogene* **2019**, *38*, 4527–4539. [[CrossRef](#)]
28. Kasaai, M. A review of several reported procedures to determine the degree of n-acetylation for chitin and chitosan using infrared spectroscopy. *Carbohydr. Polym.* **2008**, *71*, 497–508. [[CrossRef](#)]
29. Mohan, K.; Muralisankar, T.; Jayakumar, R.; Rajeevgandhi, C. A Study on structural comparisons of α -chitin extracted from marine crustacean shell waste. *Carbohydr. Polym. Technol.* **2021**, *2*, 100037. [[CrossRef](#)]
30. Zhang, L.T. Extraction of Chitin and Bio-Derived Carbonate from Waste Crab Shells Synthesis and Utilization. Master's Thesis, Nanjing Normal University, Nanjing, China, 2022. (In Chinese)
31. Feng, Z.; Yang, T.; Dong, S.; Wu, T.; Jin, W.; Wu, Z.; Wang, B.; Liang, T.; Cao, L.; Yu, L. Industrially synthesized biosafe vaterite hollow CaCO_3 for controllable delivery of anticancer drugs. *Mater. Today Chem.* **2022**, *24*, 100917. [[CrossRef](#)]
32. Zhang, C.; Li, S.; Yu, A.; Wang, Y. Nano CaCO_3 "Lysosomal bombs" enhance chemotherapy drug efficacy via rebalancing tumor intracellular pH. *ACS Biomater. Sci. Eng.* **2019**, *5*, 3398–3408. [[CrossRef](#)] [[PubMed](#)]
33. Liu, R.L.; Lian, B. Immobilisation of Cd(II) on biogenic and abiotic calcium carbonate. *J. Hazard Mater.* **2019**, *378*, 120707. [[CrossRef](#)] [[PubMed](#)]
34. Curcio, M.; Cirillo, G.; Paoli, A.; Naimo, G.D.; Mauro, L.; Amantea, D.; Leggio, A.; Nicoletta, F.P.; Iemma, F. Self-assembling dextran prodrug for redox- and pH-responsive Co-delivery of therapeutics in cancer cells. *Colloid. Surf. B* **2020**, *185*, 110537. [[CrossRef](#)] [[PubMed](#)]